Effect of soil properties on the response of pile to underground explosion

ABSTRACT

This paper develops and presents a fully coupled non-linear finite element procedure to treat the response of piles to ground shocks induced by underground explosions. The Arbitrary Lagrange Euler coupling formulation with proper state material parameters and equations are used in the study. Pile responses in four different soil types, viz, saturated soil, partially saturated soil and loose and dense dry soils are investigated and the results compared. Numerical results are validated by comparing with those from a standard design manual. Blast wave propagation in soils, horizontal pile deformations and damages in the pile are presented. The pile damage presented through plastic strain diagrams will enable the vulnerability assessment of the piles under the blast scenarios considered. The numerical results indicate that the blast performance of the piles embedded in saturated soil and loose dry soil are more severe than those in piles embedded in partially saturated soil and dense dry soil. Present findings should serve as a benchmark reference for future analysis and design.

Key words: underground explosion; pile foundation; reinforced concrete; numerical simulation

1. INTRODUCTION

Above-ground and underground explosion blast waves have been of great interest in civil engineering designs with the increase in terrorist attacks. Many studies have been carried out on the propagation of blast waves in the air, soil and rocks [1-3]. An explosion provides a sudden release of energy which produces a pressure pulse or shock wave. When a shock wave impacts a structural surface, the shock wave can cause severe structural and equipment damage, as well as personal casualties. According to past records, terrorist mainly targeted significant and iconic buildings. Therefore, it is important that these types of buildings and other infrastructure components must be shock hardened to provide safety to both occupants and equipment (or designed to provide safety to both occupants and equipment under credible blast events).

Events such as the truck bomb explosion in the World Trade Center in New York on February 26, 1993, Alfred P. Murrah Federal Building bombing incident in Oklahoma City on April 19, 1995 have caused considerable concern to researchers to investigate into the aspects of design of structures to protect the integrity of structures and their occupants from the adverse effects of bombings.

Many research projects on blast resisting designs have been carried out by the military services and the relevant documents are restricted to official use only. In the open literature, much effort has been spent in investigating the dynamic response and damage of structures to blast loading using different approaches such as analytical methods, experiments and numerical analyses. In analytical methods, the problem is solved using a theoretical model under appropriate assumed conditions. However this method is only applicable to simple problems. Small scale or prototype experiments on explosion are very expensive. They also require the use of large amount of explosives, involving risk and danger. These experiments have been mainly carried out by military services. Thus, they are typically not feasible in civilian research. With recent development of computer hardware technology, increased research in numerical simulation of partial differential equations, finite element modeling and simulations provide a viable and cost effective method for detailed investigation of blast response of the structures for different blast scenarios. Lan et al. [4] and Bao and Li [5] carried out numerical simulations using the non-linear explicit Finite Element (FE) code LS-DYNA [6] to study the dynamic response of reinforced concrete columns subjected to blast loads. Bao and Li [5] verified the numerical model through experimental studies and proposed a formula to estimate the residual axial capacity based on the mid height displacement. Xu et al. [7] presented a numerical study on the concrete spallation in reinforced concrete slabs under various blast loading conditions. Tai et al. [8] also conducted a numerical simulation study on the blast response of reinforced concrete slabs and investigated the influence of reinforcement ratio, explosive weight and standoff distance. Jayasooriya et.al [9] proposed a method to assess the vulnerability and residual capacity of building frames and components when subjected to near field blast events.

However, above previous studies mainly investigated effect of the loads induced on structural components by air propagated blast shock waves. Relatively less attention has been paid towards the blast loading on and response of foundations. Pile foundations transfer the large

loads from the superstructure above into deeper, competent soil layers which have adequate capacity to carry these loads. It follows that if these foundations are structurally damaged due to blast loading, the superstructure becomes vulnerable to failure. A foundation system can fail even if the piles are not damaged by the blast simply due to the combination of secondary action effects such as reduction of effective capacity of the pile due to blast damage, amplification of moments induced by displacements, and amplification of buckling effects. The potential damage due to blast load has not received proper attention in the current practice of pile design. Thus, design of pile foundation under dynamic lateral loads induced by blast remains a challenging issue. This is due to the lack of knowledge on assessing the response of the pile to blast load. This emphasises the need for a study to determine the blast response and vulnerability of pile foundations.

Even though researchers have not considered response of piles to blast loads, some studies on laterally loaded piles can be found in the literature. Poulos [10] analyzed the behavior of laterally loaded piles using the continuum theory. It was found that the major factors influencing the pile behavior are the pile flexibility and the length to diameter ratio, for both fixed-head and free-head piles. Budhu and Davies [11] presented a numerical analysis of single laterally loaded piles embedded in cohesion-less soil which was modeled as an elastic material. Randolph [12] studied the response of flexible pile to lateral loading using numerical simulation. He treated the soil as an elastic continuum with a linearly varying soil modulus and developed a formula to determine the maximum bending moment induced in a free-headed pile.

Although pile foundation is a surface buried structure, it can be assumed as an underground structure in some aspects. Thus, by reviewing the studies on blast response of underground structures, can be obtained valuable information such as material behavior, different analytical methods and soil-structure interaction which are useful for studying the pile foundation response subjected to blast load. The performance of underground structures subjected to blast loads is a critical research area, as these structures play an important role in the overall structure response. Underground explosions usually produce a crater, and blast-induced ground shock propagates in the surrounding soil media. If an explosion occurred near a buried structure, the soil pressure and acceleration could result in severe damage or even the collapse of the structure. The evolution of centrifuge tests had led to some studies on the

dynamic response of underground structures to blast loading [13, 14]. Shim [15] used centrifuge models to study the response of piles in saturated soil under blast loading. Shim carried out a series of 70-g centrifuge tests to investigate the blast wave propagation and response of piles embedded in saturated sand. Several tests have been carried out on Aluminium piles with hollow circular section at different standoff distances. Recently different types of numerical methods have been used to investigate the response of underground structures under blast loads. They can be classified as either uncoupled or coupled methods. In the uncoupled method, the main physical procedure is divided into different successive stages. The free field stresses are measured first and then these stresses are applied on the structure to evaluate its response. Many numerical investigations have been carried out using the uncoupled method [16, 17]. In the coupled method all the stages are included in a single model. Yang et al. [18] discussed blast resistant analysis for Shanghai metro tunnel using explicit dynamic nonlinear FE software LS-DYNA. The overall analysis evaluated the safety of the tunnel lining based on the failure criterion. Since there have not been any established common standards governing the design of such a structure, a series of parametric studies have been carried out in order to evaluate the significance of several parameters such as shear modulus and bulk modulus of soil, on the lining thrust. Nagy et al. [19] investigated the response of a buried concrete structure to various factors affecting structural performance by carrying out a parametric study using a FE model. Depths of the structure and charge were considered as parameters. It was shown that buried explosions result in significant effects on the buried structure than surface explosions under the same conditions. Anirban De [20] used fully coupled numerical model to study the effects of a surface explosion on an underground tunnel using a 3D FE model.

This paper treats the response of a single pile foundation to a buried blast loading using numerical simulations through the commercial software package LS-DYNA. The present study adopts the fully coupled numerical simulation approach employing nonlinear material models to represent the realistic behavior of the soil-pile system. The Arbitrary Lagrange Euler (ALE) formulation [21] is used in the explosion, air domain and soil region near the explosion to eliminate the distortion of the mesh under high deformation. A brief description of the background on modeling and material models is presented in the following sections in this paper. Pile foundation response to the blast loads is investigated under different soil conditions. Study on blast wave propagation in different soil types under buried explosion is

hence presented at the beginning of this paper. The response of a single pile to underground explosion is then presented. This study develops and applies comprehensive FE technique to study the blast response of a single pile foundation. It also evaluates the influence of soil properties and standoff distance on the response the reinforced concrete pile. Consequently, outcomes of this study will expand the current knowledge on the blast response of a single pile foundation and could guide as a reference for future analysis and design.

2. GROUND MOTION AND FREE-FIELD STRESSES

The study of wave propagation due to an explosion in soils can provide information useful information to engineers on the resilient characteristics of a particular site, dynamic soil structure interaction and earthquake analysis. When the explosion occurs in soil, an explosive cavity with high pressure and high temperature gas is formed. The explosive cavity immediately begins to expand against surrounding soil causing high initial radial displacements and stresses in soil that propagate outward from the explosive. In the vicinity of the explosion, stresses in the soil are extremely high and the result is that the soil will lose its shear resistance. As the explosion cavity expands, stresses in the soil decreases with distance [22].

The study of blast wave propagation in soils and validation of the soil material model are described in this section. A finite element model was developed and validated by comparing the blast wave pressures in the soils obtained from the numerical simulations with the predicted peak pressures in the manual TM5-855-1 [22]. The FE model was developed with the soil 10m high and the explosion occurring at the mid-depth of the soil. The explosive charge used in the tests was 500 kg TNT. The same modeling technique which are described in Jayasinghe et al. [23] were adopted in the present study.

2.1. Soil material model for blast study

The present study aims to investigate the blast response of a single pile embedded in different soil types. The following soil types, saturated soil, partially saturated soil and loose and dense dry soil as in Table 1 were used.

Table 1. Soil properties for numerical simulation

Upon evaluation of available soil material models in LS-DYNA, soil was modeled using FHWA [24] soil material model. This material model accounts geometrical non linearity, material non linearity, and pore water pressure development. For most soil mechanics problems, it is sufficient to use Mohr-Coulomb failure criteria. In one dimension, the yield surface of Mohr-Coulomb criterion is linear and is defined by a line between shear stress, τ, and normal stress, σ, which is written as:

$$f = \tau - (c - \sigma.\tan\phi) = 0 \qquad \text{Eq. 1}$$

Where, the constant c and ϕ are cohesion and internal friction angle of the soil, respectively. In three dimensions, the Mohr-Coulomb yield criterion is expressed as:

$$f = (\sigma_1 - \sigma_3) - (\sigma_1 + \sigma_3).\sin\phi - 2c.\cos\phi = 0 \qquad \text{Eq. 2}$$

Where, σ_1, σ_2, σ_3 are principle stresses, and σ_1 and σ_3 are maximum and minimum principle stresses.

Important advantages of the Mohr-Coulomb failure criteria include its simplicity and the fact that it permits FE solutions to be compared with a wide variety of classical plasticity solutions [25]. The Mohr-Coulomb model is the best known model for an isotropic pressure-sensitive soil. However, this model is not mathematically convenient due to the presence of corners or singularities. The surface comes to a point at the intersection with the stress axis (zero shear strength). This type of singularity can cause problems in numerical computation. To avoid such angularity, a modified Mohr-Coulomb failure criterion as described in [24], was adopted in this material model.

2.2. Prediction of free-field stresses

Ground shock propagation in soil is a complex function of the dynamic constitutive properties of the soil, the explosive products and the geometry of the explosion [1]. TM5-855-1 [22] provides the following equations to predict the peak values of pressure, velocity and acceleration, respectively.

$$P_0 = 160.f.\rho c.\left(\frac{R}{W^{1/3}}\right)^{-n} \quad \text{Eq. 3}$$

$$V_0 = 160.f.\left(\frac{R}{W^{1/3}}\right)^{-n} \quad \text{Eq. 4}$$

$$a_0 = \frac{50.f.c}{W^{1/3}}.\left(\frac{R}{W^{1/3}}\right)^{(-n-1)} \quad \text{Eq. 5}$$

In these equations, P_0 is the peak pressure in psi, V_0 is the peak particle velocity in ft/sec (fps), a_0 is the peak acceleration in g (acceleration of gravity), f is a coupling factor and is dependent on the scaled depth of the explosion, ρc is acoustic impedance in psi/fps, R is distance from the explosive source in ft, W is the charge weight in lb, c is the seismic velocity in fps, and n is an attenuation factor and is dependent on the soil type as shown in Table 2 [22].

Table 2. Soil properties for calculating ground shock parameters [22]

2.3. Comparison of numerical results for free-field stresses with TM5-855-1 predictions

As described in the above, a FE model was developed with the soil 10m high and 500kg TNT was detonated at the mid-depth of the soil. The results from the present numerical simulations for peak pressures obtained in each soil type are compared with the predicted pressures from the manual TM5-855-1 [22] to validate the soil material model for each soil type. To monitor the blast wave propagation in the soil mass, a group of target points is selected along the horizontal line to the explosive charge. The target points are located within the range 5 to 25m from the detonation point. Figure 1 shows the pressure time histories of the compressive waves at those target points in the soil type-1.

Figure 1. Pressure time histories at different distances in soil from charge for soil type-1

The peak pressures obtained in the soil type-1 from the numerical simulation are compared with the peak pressures given by TM5-855-1 [22] as shown in Figure 2. Peak pressure

attenuation has been plotted against the scaled distance in Figure 2. Since soil properties in the TM5-855-1 [22] are given in a range for considered soil type, Figure 2 shows two straight lines representing the upper empirical limit and the lower empirical limit of the peak pressure in the soil type-1. It can be noted that the numerical results for the peak pressure are almost in between the upper and lower limits of the predicted peak values for this soil type. Predicted peak pressures close to the explosion are marginally higher than the numerical results.

Figure 2. Relationship of peak pressures with scaled distance for soil type-1

Figures 3, 4 and 5 compare the peak pressures obtained from the numerical simulation with the predicted peak pressures using the TM5-855-1 for the soil types 2 to 4, respectively. As shown in those figures, the numerical results of the peak pressure attenuation agree reasonably well with empirical results. Also, the results show that attenuation of the peak pressure in the soil occurs with increasing distance from the charge.

Figure 3. Relationship of peak pressures with scaled distance for soil type-2

Figure 4. Relationship of peak pressures with scaled distance for soil type-3

Figure 5. Relationship of peak pressures with scaled distance for soil type-4

Figure 6 shows a comparison of the numerically obtained results of the peak pressure attenuations plotted against the scaled distance for all the soil types. It can be noted that the peak pressures in soil type-3 evidently shows smaller values. Soil type-1 has highest peak pressures. The small peak pressure in the dry soil results from the slow wave velocity.

Figure 6. Comparison of peak pressures attenuations

3. MODELLING THE SYSTEM: PILE-SOIL-EXPLOSIVE-AIR

Investigation of the response of the end bearing pile foundation to the ground shock caused by a buried explosion is the focus of this study. A finite element model was developed for a 10m length pile with 600mm diameter circular cross section using explicit dynamic nonlinear finite element software LS-DYNA [6]. The overall model has different regions representing the soil, air, pile and explosive charge as shown in Figure 7. By making use of symmetry, only a quarter of the system was modeled.

Figure 7. Finite element model

Except for the reinforcing cage, the eight-node solid elements were adopted for the 3D explicit analysis. The TNT explosive, the air and part of soil close to the explosive were modeled with ALE multi-material meshes. This is to prevent the element distortion in large deformations. On the other hand Lagrangian meshes were used to model the pile and the soil region away from the explosive charge. 25mm long beam elements with 2x2 Gauss integration were used for both the vertical reinforcements and ties. The vertical reinforcements were defined as Hughes-Liu beam elements with cross integration and ties were defined as truss elements.

Five kinds of materials were involved in this finite element model such as air, explosive, soil, concrete and steel. The air is commonly modeled using null material model with a linear polynomial equation of state (EOS). The TNT explosive charge is modeled using the high explosive material model with the Jones-Wilkins-Lee (JWL) equation of state. Material parameters and EOS constants for air and explosive are available in [23] and were used in the present simulations. FHWA material model was used to model the soil as described in section 2.1.

At the bottom, (the mesh of) the model was constrained in the all the directions to represent the bed rock. To form the symmetry in the FE model, the translational displacements of nodes normal to the symmetry planes were constrained. The nodes along the interfaces

between the air and soil were merged. Fixed boundary conditions were considered at the top and bottom of pile.

The interaction between the pile and surrounding soil was modeled by specifying Automatic_surface _to_surface contact option in LS-DYNA. This assumes contact at the surface and enables transfer of stresses between the solid materials. The contact nonlinearity was stablished by assigning the Viscous Damping Coefficient. In addition, static and dynamic friction coefficients were introduced to simulate the frictional forces that were transmitted across the contact interface. Thus, this contact method was used at the soil-pile interface to allow for separation in tension and ensured compatibility in compression.

A proper coupling mechanism needs to be used to achieve good interaction between concrete and reinforcement elements. There are various ways to achieve coupling in LS-DYNA such as merging the reinforcing beam elements with solid concrete elements in the form of shared nodes, which most researchers have used in their studies. In this study, the Constrained_Lagrange_in_Solid was used to couple concrete solid elements with the reinforcing cage. This method when used with the fluid-structure coupling mechanism of CTYPE = 2, couples concrete with reinforcement in an efficient manner and it removes the problem of having to align the beam nodes to the solid element nodes.

3.1. Concrete material model

The response of the concrete under dynamic loading is a complex non-linear and rate-dependent process. Concrete compressive strength is increased 200 to 300 percent at strain rates between 100 to 1000 s^{-1} [26]. Blast pressures normally produce high strain rates in the range of 100 to 10000 s^{-1}. It is well known that the numerical results are very sensitive to the material properties, and thus the ability to define the material model accurately is one of the most important issue in the numerical simulation. LS-DYNA contains several material models that can be used to represent concrete. The material model Concrete_Damage_REL3 was used in this investigation for the concrete. It is a plasticity-based model, using three shear failure surfaces and including damage and strain rate effects [27]. The advantage of this model is that unconfined compressive strength and density of concrete are the two parameters that are required in the calibration process.

In order to account for the increase in strengths under high strain rates, a coefficient called the dynamic increased factor (DIF) is employed in this analysis. The dynamic increase factor is the ratio of the strength at a point of interest on the stress strain curve under high strain rate dynamic loading to the strength at the corresponding strain under static loading. The expressions proposed by Malvar ans Crawford [28] are utilized. The DIFs for the concrete compressive strength is given as:

$$DIF = \left(\frac{\dot{\varepsilon}}{\dot{\varepsilon}_s}\right)^{1.026\alpha} \qquad \text{for } \dot{\varepsilon} \le 30s^{-1}, \qquad \text{Eq. 6}$$

$$DIF = \gamma\left(\frac{\dot{\varepsilon}}{\dot{\varepsilon}_s}\right)^{\frac{1}{3}} \qquad \text{for } \dot{\varepsilon} > 30s^{-1}, \qquad \text{Eq. 7}$$

Where $\dot{\varepsilon}$ is the strain rate in the range of 30 x 10^{-6} to 300 s^{-1}; $\dot{\varepsilon}_s$ is 30 x $10^{-6}s^{-1}$; log γ = 6.156α-2; α = 1/(5+9f_c/f_{co}); f_{co} = 10MPa; f_c is the static compressive strength of the concrete. The DIF for concrete in tension is given by:

$$DIF = \left(\frac{\dot{\varepsilon}}{\dot{\varepsilon}_s}\right)^{\delta} \qquad \text{for } \dot{\varepsilon} \le 1.0s^{-1}, \qquad \text{Eq. 8}$$

$$DIF = \beta\left(\frac{\dot{\varepsilon}}{\dot{\varepsilon}_s}\right)^{\frac{1}{3}} \qquad \text{for } \dot{\varepsilon} > 1.0s^{-1}, \qquad \text{Eq. 9}$$

Where $\dot{\varepsilon}$ is the strain rate in the range of 1 x 10^{-6} to 160 s^{-1}; $\dot{\varepsilon}_s$ is 1 x $10^{-6}s^{-1}$; log β = 6δ-2; δ = 1/(1+8f_c/f_{co}); f_{co} = 10MPa; f_c is the static compressive strength of the concrete. Thus, different rate enhancements were included in tension and compression in the concrete material model used in this study.

The erosion algorithm was used to simulate the crushing of concrete in the finite element model. When the material response in an element reaches a certain critical value, the element is immediately deleted. It gives a great means to imitate concrete spalling phenomena and produce graphical plots which are more realistic representations of the actual events. There

may be a variety of criteria governing the material erosion. In this study, the concrete elements in the pile were allowed to erode when the principle tensile strain reached 0.01 [29].

3.2. Pile reinforcement

Pile reinforcement is normally required to resist the bending and tensile stresses, but may be used to carry a portion of the compression load. 20mm diameter 16 number of bars were used as the pile vertical reinforcement in this study. 10mm diameter steel bars were used for the transverse reinforcements. Transverse reinforcement ratio of 0.24% was used in piles provided at a spacing of 200mm. Beam elements with 2x2 Gauss integration were used to model the both vertical and transverse reinforcements in the reinforced concrete pile in this analysis. Reinforcements were modeled as elastic perfectly-plastic materials using the plastic kinematic model available in the LS-DYNA. Kinematic hardening with strain rate effects was implemented for the reinforcement. Strain rate is accounted for using the Cowper-Symonds model given by [6]

$$\frac{\sigma_d^{'}}{\sigma_s} = 1 + \left(\frac{\dot{\varepsilon}}{C} \right)^{1/P} \qquad \text{Eq. 10}$$

In the above equation, σ'_d is the dynamic flow stress at a uni-axial plastic strain rate $\dot{\varepsilon}$, and σ_s is the associated static flow stress. C and P represent the material constants. Material model parameters for steel is listed in Table 3.

Table 3. Material model parameters for main reinforcement and ties [30]

4. BLAST RESPONSE OF PILE IN DIFFERENT SOIL TYPES

This study investigated the response and damage of the (10m long) end bearing Reinforced Concrete (RC) single pile when subjected blast loads for a standoff distance of 7.5m in different soil types. As shown in Table 1, four soil types were considered: saturated soil, partially saturated soil, loose dry soil and dense dry soil, labelled as soil types 1,2,3 and 4.

Figure 8 shows the time histories of the horizontal deformation of the pile embedded in different soils. Pile deformations are presented at three heights from the pile tip: 2.5m (point A), 5m (point B) and 7.5m (point C). This Figure demonstrates that the pile has residual deflection in all the cases. These residual deflections show the occurrence of the plastic deformation of the pile and indicate that the pile has suffered permanent deformation under the buried blast. For the parameters considered in this study, it can be noted that the pile embedded in soil type-3 has the highest pile deformation and when it embedded in the soil type-2 it has the lowest pile deformation. The pile embedded in soil type-1 was found to have a maximum horizontal residual deflection of 369 mm, and maximum lateral residual deflection of 247 mm was observed in the soil type-2. Also, it was found that the piles embedded in the soil types 3 and 4 have maximum residual deflections of 400mm and 370mm, respectively.

The damage to the reinforced concrete is also observed for the pile embedded in all soil types. Figure 9 depicts the concrete effective plastic strain variation of the piles with the element erosion that were that observed on the pile for a stand-off distance of 7.5m. Effective plastic strain is the damage parameter in concrete_damage_rel3 material model which range from 0 to 2. Elastic state of the concrete is represented by 0 with blue color and the yielding and post yielding in incorporated within 0 to 2. The residual capacity of the concrete is indicated by 2. As can be seen, it is clear that pile was critically damaged in all the cases. Concrete elements have eroded in the top end of the pile in all the cases. This indicates that the concrete at the top end of the pile was totally destroyed in all the cases. Reinforcements were found to have severely deformed at the top end. Figure 9(a) shows that concrete in the bottom end was also severely damaged in the pile embedded in the soil type-1. It can be noted that the pile embedded in the soil type-1 suffered the most damage compared to the other two piles. However concrete in the middle of the pile suffered most damage in the pile embedded in the soil type-3.

Figure 8. Pile deformation (a) in soil type-1 (b) in soil type-2 (c) in soil type-3 (d) in soil type-4

Figure 9. Pile damage (a) in soil type-1 (b) in soil type-2 (c) in soil type-3 (d) in soil type-4

From the above results for pile deformations and pile damage, it can be concluded that under the same buried explosion, piles embedded in soil type-1 or soil type-3 suffer more damage than piles embedded in soil type-2 and soil type-4. As seen in the Figure 6, blast wave pressures are high in the soil type-1 and this could be the reason for the severe damage in the embedded pile. Even though blast wave pressures are lower in soil type-3 as seen in Figure 6, the displacement of the soil could be high due to the poor bond between the soil particles. This could therefore be the reason for the severe deformation of the pile embedded in soil type-3 under the buried explosion.

4.1. Effect of the standoff distance

As described in the section 2, blast wave pressures in the soil decrease with increase of distance from the charge. Thus, using the proposed numerical method, further studies were carried out to investigate the effect of standoff distance on the blast response of pile embedded in different soil types. In this section, pile deformation and damage are presented for the standoff distances of 10m and 15m from the explosive.

In Figure 10, the time histories of the horizontal deformations of the pile at three heights from the pile tip: 2.5m (point A), 5m (point B) and 7.5m (point C) are presented for the standoff distance 10m from the explosion. It also demonstrates that the piles have suffered permanent deformation under the buried blast. It can be noted that the pile embedded in the soil type-3 has highest pile deformation and when it embedded in the soil type-2 it has the lowest pile deformation. The pile embedded in the soil type-1 was found to have a maximum horizontal residual deflection of 165 mm, and maximum lateral residual deflection of 157 mm was observed in the soil type-2. Also, it was found that the piles embedded in the soil types 3 and 4 had deflected 280mm and 270mm, respectively. Figure 11 shows the concrete effective plastic strain variation of the pile with the element erosion that was observed on the pile for a stand-off distance of 10m. It is clear that piles were critically damaged in all the cases as same as in the stand-off distance of 7.5m. As expected, pile damages and deformations have decreased. In this case also, piles embedded in the soil type-1 and in the soil type-3 suffered more damage than piles embedded in the soil types 2 and 4. However, deformed shape of the

pile embedded in the soil type-3 is different to that in the previous case (stand-off distances of 7.5m).

Figure 10. Pile deformation for standoff distance 10m (a) in soil type-1 (b) in soil type-2 (c) in soil type-3 (d) in soil type-4

Figure 11. Pile damage for standoff distance 10m (a) in soil type-1 (b) in soil type-2 (c) in soil type-3 (d) in soil type-4

Figure 12 shows the concrete effective plastic strain variation of the piles with the element erosion that were observed on the pile for a stand-off distance of 15m. In this case also, concrete in the top and bottom ends of the pile embedded in the soil type-1 were totally destroyed. Maximum lateral deformation of 85mm was found in the pile. Spalling was also observed at the top ends of the piles embedded in the soil types 2, 3 and 4. The pile embedded in the soil type-2 was found to have a maximum horizontal residual deflection of 54 mm, and it was found that the piles embedded in soil types 3 and 4 had deflected 80mm and 75mm, respectively. Although the pile embedded in the soil type-3 had larger deformations than other three cases for the standoff distances 7.5m and 10m, the pile embedded in the soil type-1 has deformed more for the standoff distance 15m.

Figure 12. Pile damage for standoff distance 15m (a) in soil type-1 (b) in soil type-2 (c) in soil type-3 (d) in soil type-4

5. SUMMARY

A coupled numerical model was used to study the dynamic response of reinforced concrete pile foundation to a buried explosion using the commercial computer program LS-DYNA. This study investigated the blast response of a single pile embedded in several soil types: saturated soil, partially saturated soil, loose dry soil and dense dry soil. Soil was modeled using FHWA soil material model, blast wave propagation in soils was validated with the predicted pressures using the TM5-855-1. Horizontal pile deformation and damages on the pile were obtained from the numerical simulations. Based on the parameters considered in the study and the presented results, the following main conclusions can be drawn.

1. Performance of the piles embedded in saturated soil and loose dry soil are more severe than that in pile embedded in partially saturated soil and dense dry soil when subjected to the same buried explosion.

2. Since blast wave pressures are high in saturated soil, they cause severe damage in the pile. Even though blast wave pressures are small in loose dry soil, the displacement of the soils might be high due to the poor bond between soil particles. This might therefore be the reason for the severe deformation of the pile embedded in loose dry soil under buried explosion

3. Pile damages and deformations decrease with the distance from the explosive.

4. For scaled distances 1 and 1.3 $m/kg^{1/3}$, the pile embedded in the loose dry soil has the maximum pile deformation.

5. For scaled distance 1.9 $m/kg^{1/3}$, the pile embedded in the saturated soil has the maximum pile deformation.

6. The modeling techniques developed in this paper and the outcomes of the study increase our understanding in this area and could be useful in future studies.

6. REFERENCES

[1] J.L. Drake, and C.D. Little, Ground shock from penetrating conventional weapons, Proc. 1st Symp. On the interaction of non-nuclear munitions with structures, US Air force academy, CO, 1983, pp 1-6.

[2] P.S. Westine, and G.J. Friensenhahn, Free-field ground shock pressure from buried detonations in saturated and unsaturated soils, Proc. 1st Symp. On the interaction of non-nuclear munitions with structures, US Air force academy, CO, 1983, pp 12-16.

[3] C. Wu, Y. Lu, and H. Hao, Numerical prediction of blast induced stress wave from large scale underground explosion, International journal for numerical and analytical methods in geomechanics, 28 (2004), pp 93-109.

[4] S. Lan, J.E. Crawford, and K.B. Morrill, Design of reinforced concrete columns to resist the effects of suitcase bombs, International proceeding of 6th international conference on shock and impacts loads on structures, Australia, 2005, pp 5-10.

[5] X. Bao, and B. Li, Residual strength of blast damaged reinforced concrete columns, International Journal of Impact Engineering, 37 (3) (2010), pp 295-308.

[6] LS-DYNA, Livermore software technology cooperation, LS-DYNA user's manual, version 971, 2007.

[7] K. Xu, and Y. Lu, Numerical simulation study of spallation in reinforced concrete plates subjected to blast loading. Computers and structures, 84 (5-6) (2006), pp 431-438.

[8] Y.S. Tai, T.L. Chu, H.T. Hu, and J.Y. Wu, Dynamic response of a reinforced concrete slab subjected to air blast load, Theoretical and applied fracture mechanics, 56 (2011), pp 140-147.

[9] R. Jayasooriya, D.P. Thambiratnam, N. Perera, and V. Kosse, Blast and residual capacity analysis of reinforced concrete framed buildings, Engineering structures, 33 (12) (2011), pp 3483-3495.

[10] H.G. Poulos, Behavior of laterally loaded piles: I – single pile, JSMFE, ASCE, 97 (SM5) (1991), pp 711-731.

[11] M. Budhu, T.G. Davies, Nonlinear analysis of laterally loaded piles in cohesionless soils, Canadian geotechnical jouranal, 24 (2) (1987), pp 289-296.

[12] M.F. Randolph, The response of flexible piles to lateral loading, Geotechnique, 31 (2) (1981), pp 247-259.

[13] H. Tabatabai, Centrifuge modeling of underground structures subjected to blast loading, PhD Thesis, Department of Civil Engineering, University of Florida, 1987.

[14] A. De, T.F. Zimmie, T. Abdoun, and A. Tessari, Physical modeling of explosive effects on tunnels, Fourth international symposium on tunnel safety and security, Frankfart am Main, Germany, March 2010, pp 159-167.

[15] H-S. Shim, Response of piles in saturated soil under blast loading, Doctoral thesis, University of Colorado, Boulder, US, 1996.

[16] Z. Yang, Finite element simulation of response of buried shelters to blast loadings, Finite element in analysis and design, 24 (3) (1997), pp 113-132.

[17] M.W. Gui, and M.C. Chien, Blast-resistant analysis for a tunnel passing beneath Taipei Shongsan airport- a parametric study, Geotechnical and geological engineering, 24 (2006), pp 227-248.

[18] Y. Yang, X. Xie, and R. Wang, Numerical simulation of dynamic response of operating metro tunnel induced by ground explosion, Journal of rock mechanics and geotechnical engineering, 2 (4) (2010), pp 373-384.

[19] N.M. Nagy, E.A. Eltehawy, H.M. Elhanafy, and A. Eldesouky, Numerical modeling of geometrical analysis for underground structures, 13th International conference on aerospace science and aviation technology, Egypt, May 2009.

[20] Anirban De, Numerical simulation of surface explosions over dry, cohesionless soil, Computers and Geotechnics, 43 (2012), pp 72-79.

[21] Hallquist, J.O. LS-DYNA Theoretical Manual - Nonlinear Dynamic Analysis of Structures, Livermore, California: Livermore Software Technology Corporation, Livermore, California, 1998.

[22] TM5-855-1, Fundamental of protective design for conventional weapons, US Army technical manual, 1986

[23] L.B. Jayasinghe, D.P. Thambiratnam, N. Perera, and J.H.A.R. Jayasooriya, Computer simulation of underground blast response of pile in saturated soil, Computers and Structures, 120 (2013), pp 86-95.

[24] B.A. Lewis, Manual for LS-DYNA soil material model 147, Federal Highway Administration, FHWA-HRT-04-095, McLean, VA, 2004.

[25] A.J. Abbo, and S.W. Sloan, A smooth hyperbolic approximation to the Mohr-Coulomb yield criterion, Computer and structures, 54 (3) (1995), pp 427-441.

[26] C.A. Ross, J.W. Tedesco, and S.T. Kuennen, Effects of strain rate on concrete strength, ACI material journal, 30 (1995), pp 54-62.

[27] L.J. Malvar, J.E. Crawford, J.W. Wesevich, and D.A. Simons, A plasticity concrete material model for DYNA3D, International journal of impact engineering, 19 (9-10) (1997), pp 847-873.

[28] L.J. Malvar, J.E. Crawford, and K.B. Morrill, K and C concrete material model, release III – automated generation of material model input, Karagozian and Case structural engineers, Technical report 2000 TR-99-24.3.

[29] Y.S. Tai, T.L. Chu, H.T. Hu, and J.Y. Wu, Dynamic response of a reinforced concrete slab subjected to air blast load, Theoretical and applied fracture mechanics, 56 (2011), pp 140-147.

[30] H.M.I. Thilakarathna, D.P. Thambiratnam, M. Dhanasekar, and N. Perera, Numerical simulation of axially loaded concrete columns under transverse impact and vulnerability assessment, International Journal of Impact Engineering, 37 (11) (2010), pp 1100-1112.

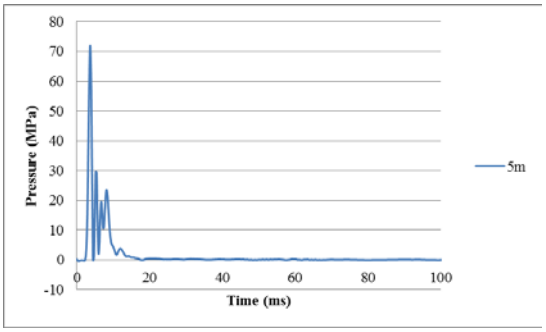
80
70
60
50
40
30
20
10
0
-10
Pressure (MPa)
0
20
40
60
80
100
Time (ms)
5m

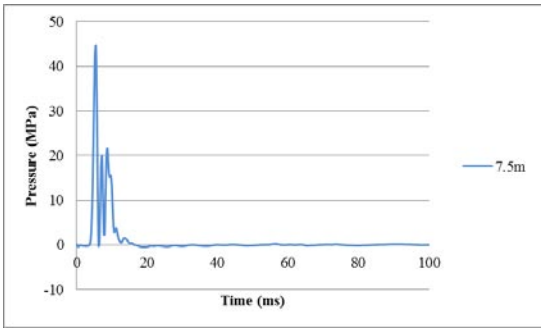
50
40
30
20
10
0
-10
Pressure (MPa)
0
20
40
60
80
100
Time (ms)
7.5m

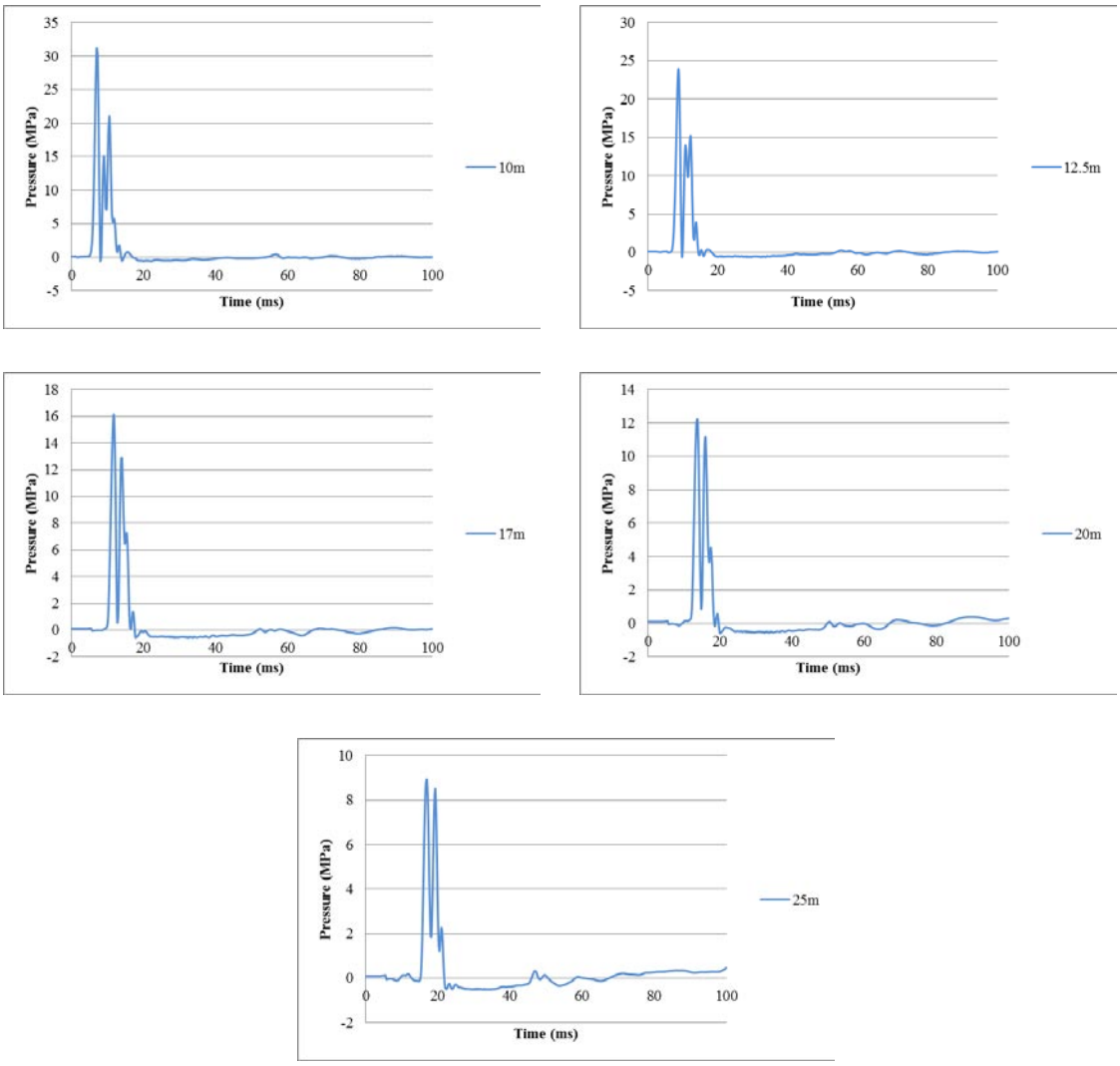

Figure 1. Pressure time histories at different distances in soil from charge for soil type-1

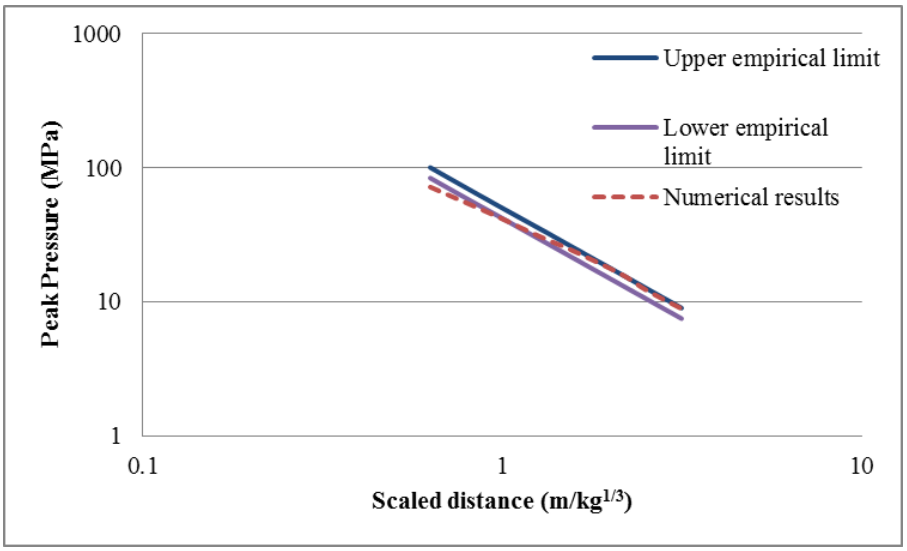

Figure 2. Relationship of peak pressures with scaled distance for soil type-1

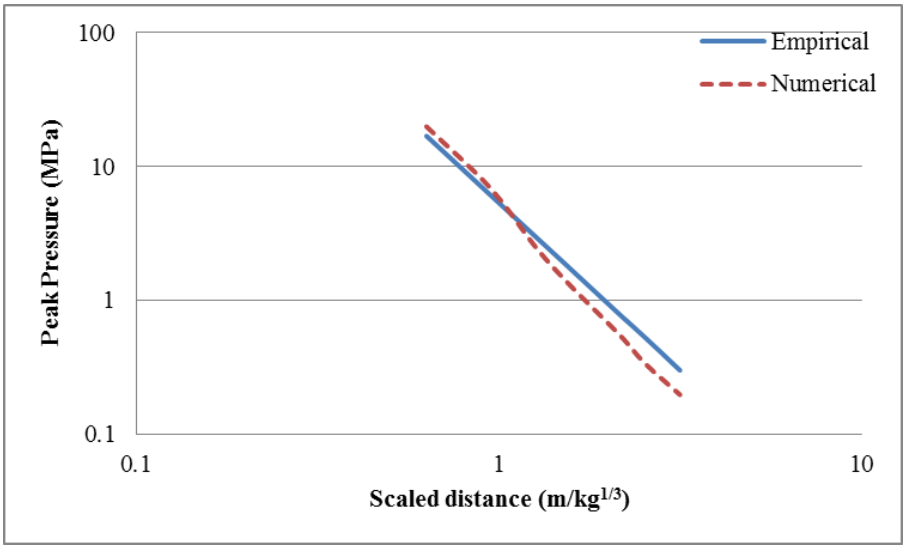

Figure 3. Relationship of peak pressures with scaled distance for soil type-2

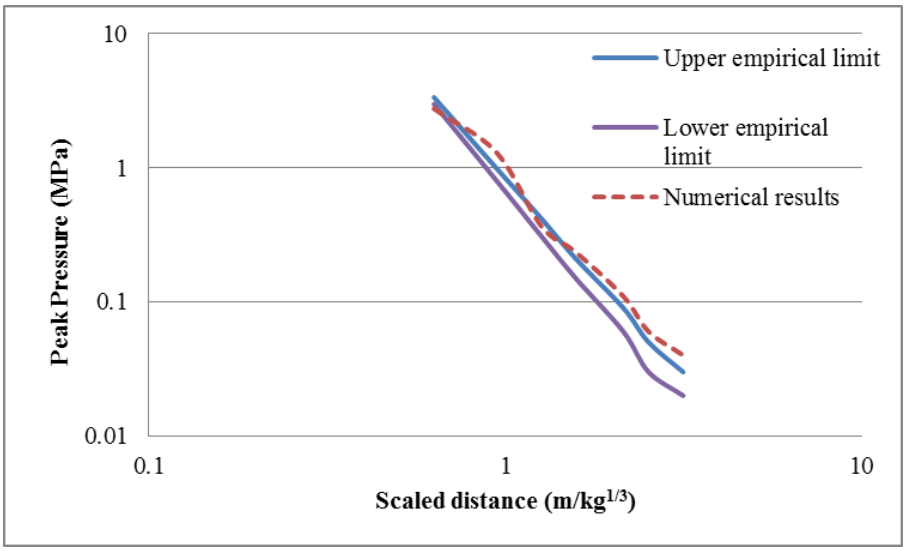

Figure 4. Relationship of peak pressures with scaled distance for soil type-3

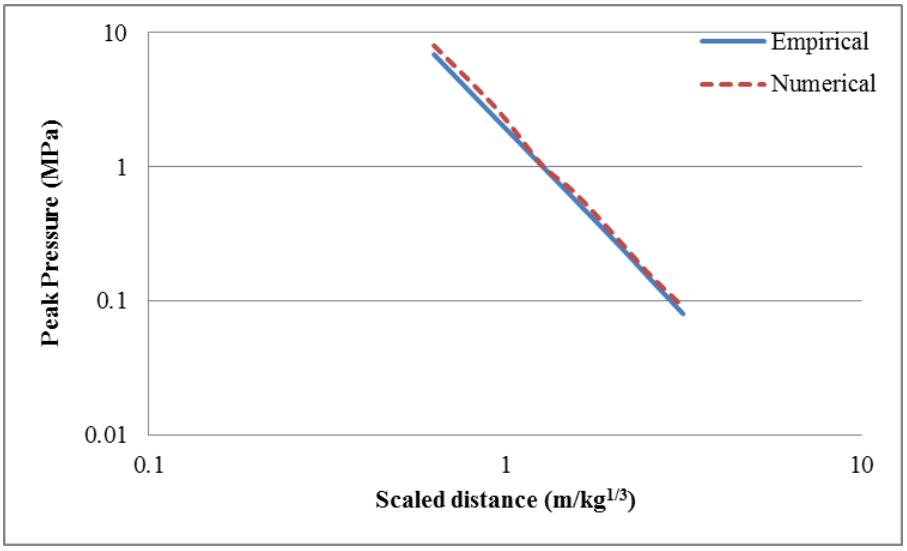

Figure 5. Relationship of peak pressures with scaled distance for soil type-4

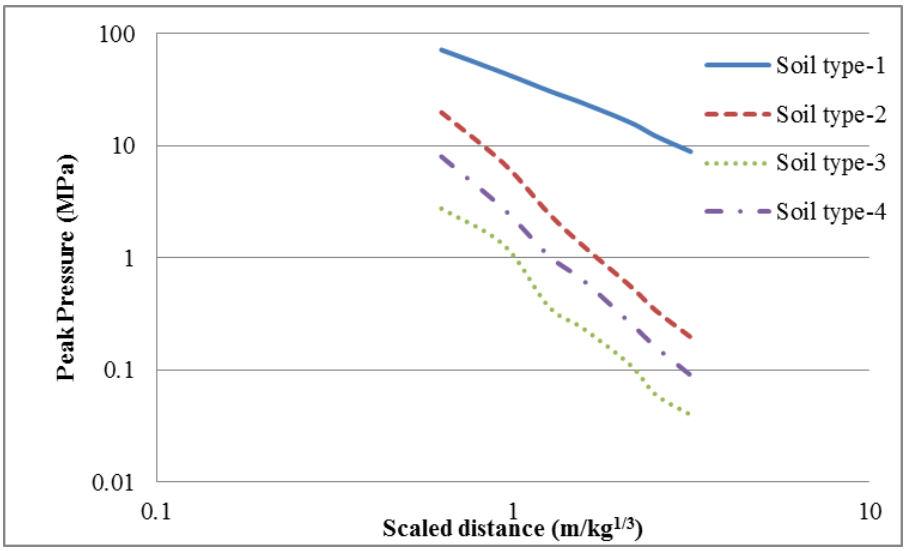

Figure 6. Comparison of peak pressures attenuations

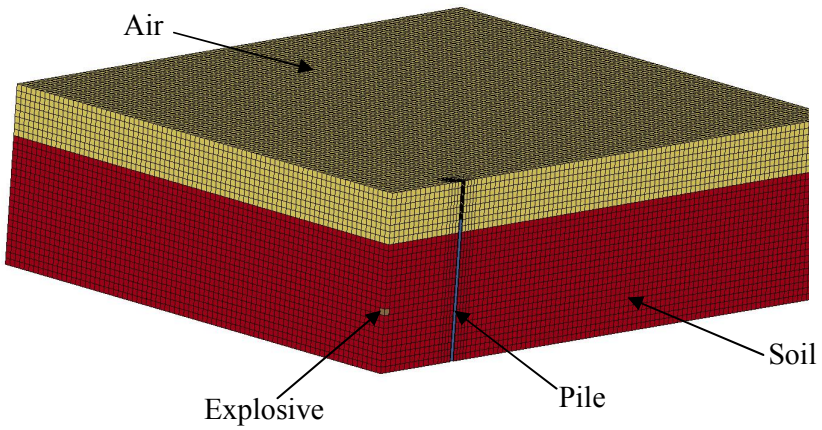

Figure 7. Finite element model

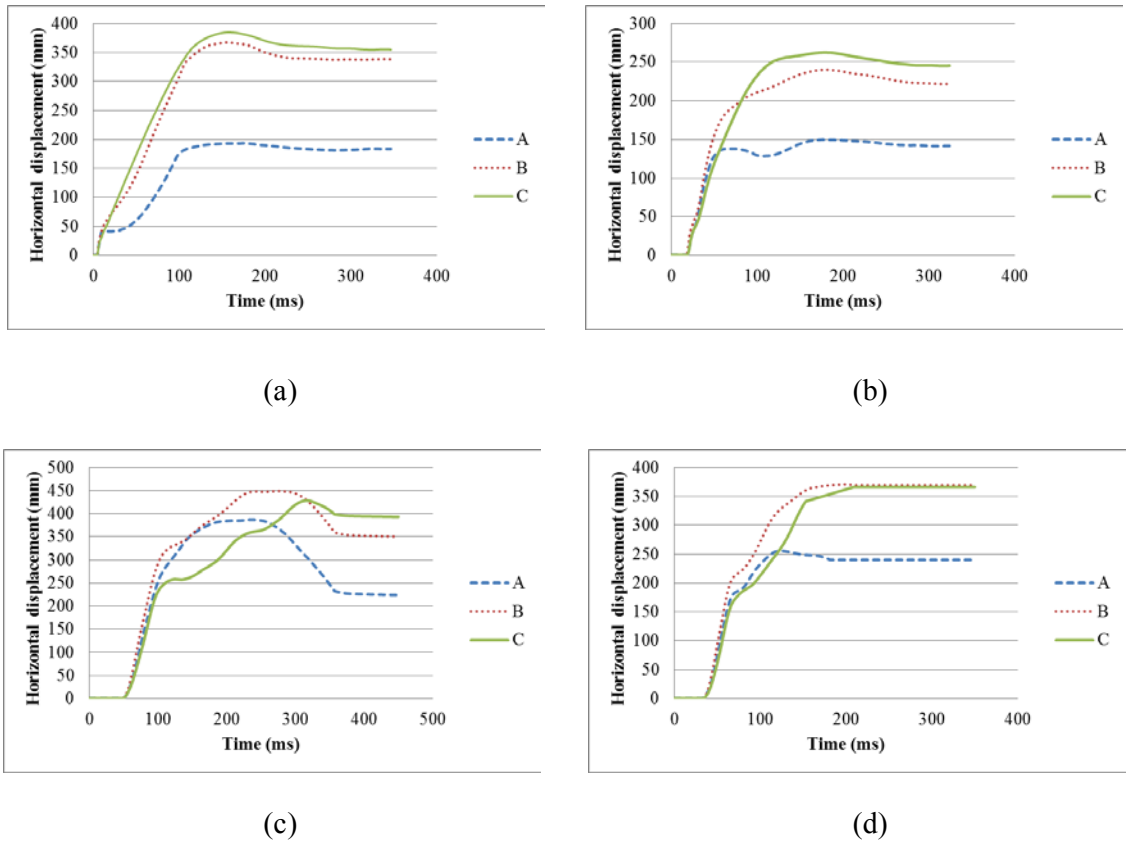

Figure 8. Pile deformation (a) in soil type-1 (b) in soil type-2 (c) in soil type-3 (d) in soil type-4

(a) (b)

(c) (d)

Figure 9. Pile damage (a) in soil type-1 (b) in soil type-2 (c) in soil type-3 (d) in soil type-4

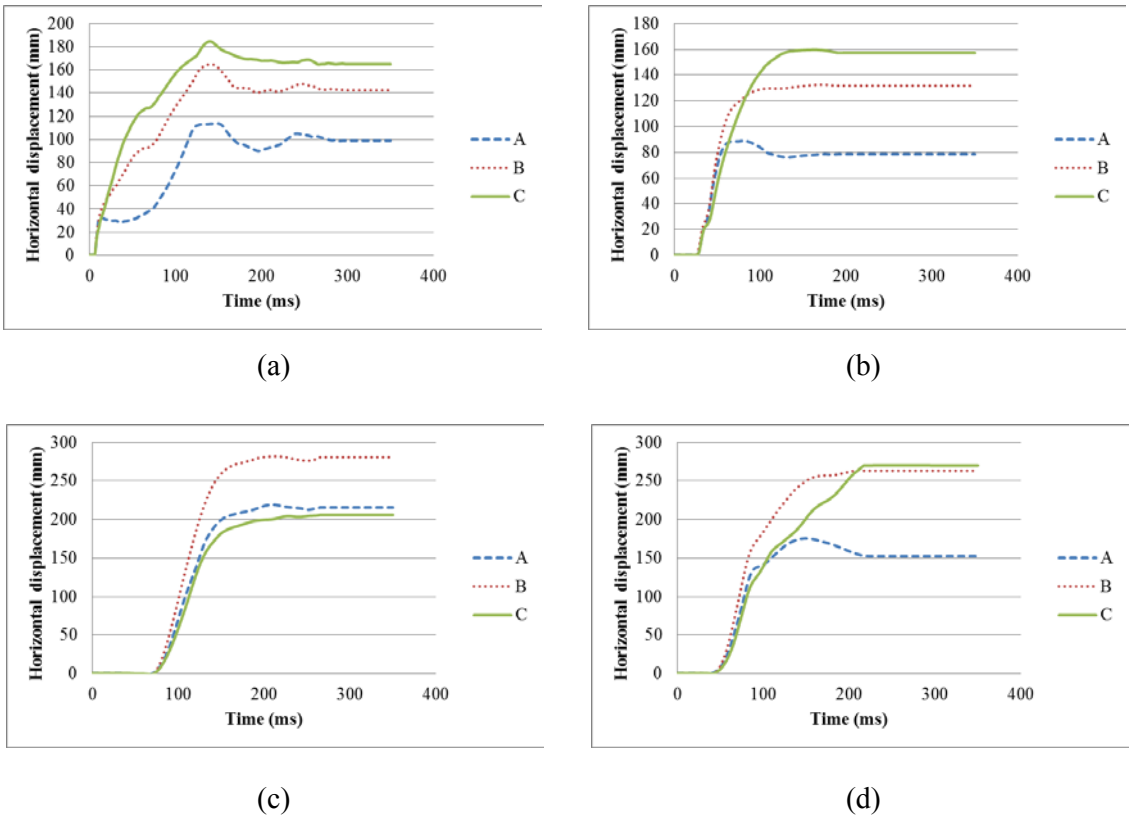

Figure 10. Pile deformation for standoff distance 10m (a) in soil type-1 (b) in soil type-2 (c) in soil type-3 (d) in soil type-4

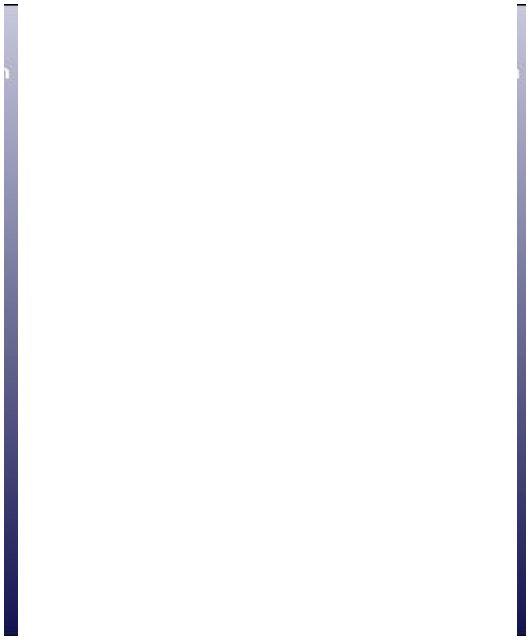

(a) (b)

(c) (d)

Figure 11. Pile damage for standoff distance 10m (a) in soil type-1 (b) in soil type-2 (c) in soil type-3 (d) in soil type-4

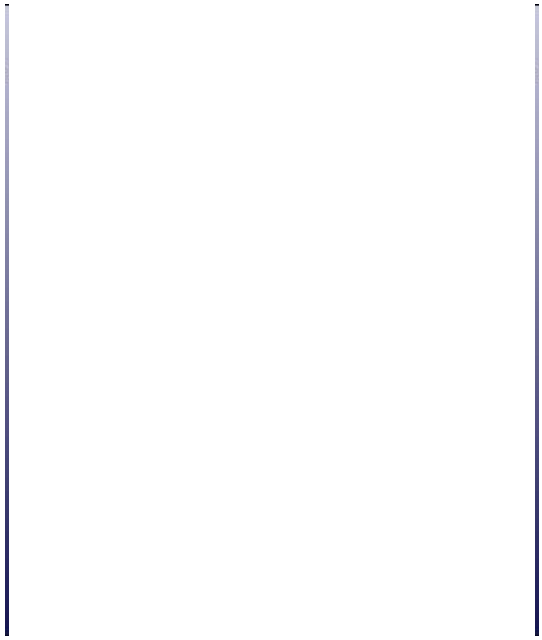

(a) (b)

(c) (d)

Figure 12. Pile damage for standoff distance 15m (a) in soil type-1 (b) in soil type-2 (c) in soil type-3 (d) in soil type-4

Table 1. Soil properties for numerical simulation

	Soil type 1	Soil type 2	Soil type 3	Soil type 4
Soil type	Saturated soil	Partially saturated soil	Loose dry soil	Dense dry soil
Composition	Clay	Sand & Clay	Sand	Sand
Density	2065 kg/m^3	1960 kg/m^3	1450 kg/m^3	1800 kg/m^3
Degree of saturation	100%	85% (volume of air > 4%)	0%	0%
Seismic velocity	1575 m/s	500 m/s	175 m/s	300 m/s

Table 2. Soil properties for calculating ground shock parameters [22]

Soil types	Unit weight, (kg/m^3)	Seismic velocity, c (m/s)	Acoustic impedance, ρc (MPa.s/m)	Attenuation coefficient, n
Heavy saturated clays and clay shale	1920 - 2080	> 1524	33.9 – 40.7	1.5
Saturated sandy clays and sands with air voids < 1%	1760 - 1984	1524	29.4	2.25 - 2.5
Dense sand with high relative density	1744	488	9.9	2.5
Wey sandy clay with air voids > 4%	1920 - 2000	549	10.8	2.5
Sandy loam, loess, dry sands and backfills	1984	305	5	2.75
Loose, dry sands and gravels with low relative density	1440 - 1600	183	2.7	3 - 3.25

Table 3. Material model parameters for main reinforcement and ties [30]

	Density (kg/m^3)	Young's modulus (GPa)	Poission's ratio	Yield stress (MPa)	Tangent modulus (GPa)	Hardening Parameter (β)	C	P
Vertical R/F	7800	210	0.3	548	2	0	40	5
Ties	7800	210	0.3	350	2	0	40	5